
# MIT Sloan School of Management

**Working Paper 4228-01**
**December 2001**

## A MATHEMATICAL MODEL OF THE IMPACT OF NOVEL TREATMENTS ON THE Aß BURDEN IN THE ALZHEIMER'S BRAIN, CSF AND PLASMA

Lawrence M. Wein, David L. Craft, Dennis J. Selkoe

# A Mathematical Model of the Impact of Novel Treatments on the A$\beta$ Burden in the Alzheimer's Brain, CSF and Plasma

David L. Craft[1], Lawrence M. Wein[2*], Dennis J. Selkoe[3]

[1]*Operations Research Center, MIT, Cambridge, MA 02139*

[2]*Sloan School of Management, MIT, Cambridge, MA 02139*

[3]*Center for Neurologic Diseases, Harvard Medical School, Brigham and Women's Hospital, Boston, MA 02115*

*Person to whom correspondence should be addressed; email: lwein@mit.edu

**Abstract**

With the advent of novel therapies for AD, there is a pressing need for biomarkers that are easy to monitor, such as the amyloid-beta ($A\beta$) levels in the cerebrospinal fluid (CSF) and plasma. To gain a better understanding of the explanatory power of these biomarkers, we formulate and analyze a compartmental mathematical model for the $A\beta$ accumulation in the brain, CSF and plasma throughout the course of Alzheimer's treatment. Our analysis reveals that the total $A\beta$ burden in the brain is dictated by a unitless quantity called the polymerization ratio, which is the product of the production and elongation rates divided by the product of the fragmentation and loss rates. In this ratio, the production rate and loss rate include a source and sink term, respectively, related to the inter-compartmental transport. Our results suggest that production inhibitors are likely to reduce the $A\beta$ levels in all three compartments. In contrast, agents that ingest monomers off of polymers, or that increase fragmentation or block elongation, may also reduce $A\beta$ burden in the brain, but may produce little change in – or even transiently increase – CSF and plasma $A\beta$ levels. Hence, great care must be taken when interpreting these biomarkers.

## Introduction

Amyloid-beta (A$\beta$) polymerization and plaque deposition are central to the pathogenesis of Alzheimer's disease (AD)[1]. Several novel treatments, such as the enhancement of A$\beta$ clearance by an A$\beta$ vaccine[2–4] and the reduction of A$\beta$ production by a $\gamma$-secretase inhibitor[5, 6], have shown promise in preclinical studies. While cognitive tests will provide the ultimate assessment of the efficacy of these and other agents[7], it will still be important to estimate the A$\beta$ burden in the brain. As these therapies enter clinical trials, a key challenge will be to infer treatment-induced changes in the A$\beta$ burden in the brain from the A$\beta$ levels in more easily monitored compartments, such as the cerebrospinal fluid (CSF) and the plasma. These inferences need to be based on a solid understanding of the A$\beta$ kinetics throughout the three interrelated compartments. Although the transport of A$\beta$ between the various compartments has been studied in recent years[8–12], the impact of treatment on the A$\beta$ kinetics in these three compartments has not been elucidated.

In previous work[13], we formulated and analyzed a mathematical model that tracks the dynamics of A$\beta$ production and loss, and polymer elongation and fragmentation in the brain during the course of treatment. Here we generalize these results by considering a three-compartment model, where A$\beta$ is transported between the brain, CSF and plasma. Simple formulas and numerical results are presented that provide some insights into system behavior, and that can be used to estimate key transport, production and clearance parameters as new clinical data becomes available.

### Mathematical model

We focus on A$\beta_{42}$ (the 42 amino-acid form of A$\beta$), which is the primary ingredient in parenchymal plaques[14]. If we assumed that each brain polymer consisted of only A$\beta_{40}$ or A$\beta_{42}$, then the model could also be applied to A$\beta_{40}$, which produces

cerebrovascular deposits[8, 10]; however, we do not pursue this avenue here, and for ease of notation refer to $A\beta_{42}$ simply as $A\beta$. We also only consider extracellular $A\beta$, which is likely to be in a dynamic equilibrium with intracellular $A\beta$. Because we are primarily interested in the total $A\beta$ burden in the three compartments, as opposed to the number and size of plaques, we restrict our attention to $A\beta$ polymerization, and do not attempt to capture the downstream processes of fibrillization or plaque formation. While different parts of the brain have markedly different $A\beta$ levels[16], these levels tend to change proportionately and hence we model the brain as a single homogeneous compartment. Finally, because diffusion through extracellular spaces in the brain is much faster than transport across the blood-brain barrier (BBB)[15], we can safely assume homogenous mixing within the CSF and plasma.

Our model is an infinite system of nonlinear ordinary differential equations that are related to a large class of models used to study actin formation[17], polymer chemistry[18], and galaxy formation, crystallization and cloud formation[19–20]. While the polymerization and depolymerization processes we employ are specialized to AD and are less general than many considered in the literature, the main novelty of our model is the incorporation of multiple compartments with sources (production) and sinks (loss).

For ease of understanding, nearly all of our mathematical notation is mnemonic. For $i = 1, 2, \ldots$, we let $b_i(t)$ be the concentration of $A\beta$ i-mers at time $t$. Because very few oligomers have been found in the CSF[21] or plasma, we assume that $A\beta$ appears in the CSF and plasma only as monomers, and denote their time-dependent concentrations by $c(t)$ and $p(t)$, respectively.

The differential equations specify the time rate of change of these concentrations,

denoted by $\dot{b}_i(t)$, $\dot{c}(t)$ and $\dot{p}(t)$, and are given by

$$\underbrace{\dot{b}_1(t)}_{\substack{\text{brain A}\beta \\ \text{monomers}}} = \underbrace{p_b}_{\text{production}} + \underbrace{f\sum_{i=2}^{\infty} b_i(t)}_{\text{all fragmentations}} - \underbrace{eb_1(t)\big(2b_1(t)+\sum_{i=2}^{\infty} b_i(t)\big)}_{\text{all elongations}} + \underbrace{\sum_{x=\{p,c\}} r_{xb}x(t)}_{\substack{\text{monomers from} \\ \text{plasma and csf}}} - \underbrace{\sum_{x=\{p,c\}} r_{bx}b_1(t)}_{\substack{\text{monomers to} \\ \text{CSF and plasma}}} - \underbrace{l_b b_1(t)}_{\substack{\text{loss (e.g., by} \\ \text{degradation)}}} \quad (1)$$

$$\underbrace{\dot{b}_i(t)}_{\substack{\text{brain A}\beta \\ (i)\text{-mers}}} = \underbrace{eb_1(t)b_{i-1}(t)}_{\substack{\text{elongation} \\ \text{of } (i-1)\text{-mers}}} + \underbrace{fb_{i+1}(t)}_{\substack{\text{fragmentation} \\ \text{of } (i+1)\text{-mers}}} - \underbrace{eb_1(t)b_i(t)}_{\substack{\text{elongation} \\ \text{of } i\text{-mers}}} - \underbrace{f(1-\frac{1}{2}\mathrm{I}_{\{i=2\}})b_i(t)}_{\substack{\text{fragmentation} \\ \text{of } i\text{-mers}}}, \quad (2)$$

$$\underbrace{\dot{c}(t)}_{\text{CSF A}\beta} = \underbrace{p_c}_{\text{production}} + \underbrace{\sum_{x=\{b,p\}} r_{xc}x(t)}_{\substack{\text{monomers from} \\ \text{brain and plasma}}} - \underbrace{\sum_{x=\{b,p\}} r_{cx}c(t)}_{\substack{\text{monomers to} \\ \text{brain and plasma}}} - \underbrace{l_c c(t)}_{\text{loss}}, \quad (3)$$

$$\underbrace{\dot{p}(t)}_{\text{plasma A}\beta} = \underbrace{p_p}_{\text{production}} + \underbrace{\sum_{x=\{b,c\}} r_{xp}x(t)}_{\substack{\text{monomers from} \\ \text{brain and CSF}}} - \underbrace{\sum_{x=\{b,c\}} r_{px}p(t)}_{\substack{\text{monomers to} \\ \text{brain and csf}}} - \underbrace{l_p p(t)}_{\text{loss}}. \quad (4)$$

The model is also depicted in Figure 1. In equation (1), A$\beta$ monomers in the brain are produced by cleavage of the amyloid precursor protein (APP) at the constant rate $p_b$. These monomers live for $l_b^{-1}$ time units on average before being lost, e.g., via cell internalization or protease degradation. Similar production and loss terms appear in equations (3) and (4). Equations (1)-(2) assume that elongation occurs only by monomer addition with elongation constant $e$ (i.e., $eb_1(t)b_{i-1}(t)$ is the rate that $(i-1)$-mers elongate to $i$-mers), and that fragmentation occurs only by monomer break-offs at rate $f$ (i.e., $i$-mers fragment into an $(i-1)$-mer and a monomer at rate

$fb_i(t)$). The factor 2 in front of $b_1(t)$ in equation (1) arises because the elongation of a dimer requires 2 monomers. The indicator variable $I_{\{i=2\}}$ equals 1 if $i = 2$ and equals 0 otherwise; the factor $\frac{1}{2}$ in front of $I_{\{i=2\}}$ is due to the fact that a dimer can only fragment in one location, whereas larger $i$-mers possess two potential fragmentation sites.

An alternate modeling approach, which is pursued later in the paper, is to allow direct clearance of monomers off of $i$-mers (e.g., to represent microglial ingestion of polymers), rather than requiring a two-step procedure of monomer fragmentation followed by monomer clearance. This alternative would result in the omission of the "all fragmentations" term in equation (1) and the re-interpretation of $f$as an ingestion rate, and gives qualitatively similar results[13].

The remaining terms in the model describe the intercompartmental transport, which is typically some combination of passive diffusion and active or carrier-mediated transport. Although CSF→plasma and plasma→brain transport are likely dominated by active transport, we assume that all transport rates are first-order, rather than obeying Michaelis-Menten kinetics[22]; the rate from compartment $i$ to compartment $j$ is denoted by $r_{ij}$ for $i, j = b, c$ or $p$. Our main reason for this simplification is that it eases the parameter estimation task. However, the A$\beta$ levels in these three compartments do not undergo many orders-of-magnitude changes during the course of treatment; hence, the saturation effect may be minor in the practically relevant range.

Finally, we note that most of plasma A$\beta$ is bound, primarily to albumin[23, 24]. Similarly, CSF A$\beta$ binds to gelsolin[25]. Moreover, it is not yet understood whether bound or free A$\beta$, or both, gets transported across the BBB[11]. To confuse matters further, many laboratory and clinical studies that report plasma A$\beta$ values quantify only free A$\beta$[23]. Here, we implicitly assume that linear (i.e., unsaturated) binding occurs (i.e., free and total A$\beta$ are in direct proportion[22]) and that there is a linear relationship between the total A$\beta$ and its clearance rate out of the plasma. There-

fore when we model free monomers entering the plasma, it is understood that a proportion of them bind to plasma proteins but that this binding does not affect the linear degradation and transport laws applied to the total A$\beta$.

# Results

## Steady-state solution

The steady-state analysis of equations (1)-(4) consists of setting the left sides of these equations to zero and solving for the steady-state A$\beta$ levels $b_i$, $c$ and $p$; the details of the derivation are omitted. To present our results in a transparent manner, we first determine the *effective* production and loss rates for each compartment, which augment the actual rates by incorporating monomer exchange with the other two compartments. Because only monomers are transported between compartments, by symmetry it suffices to index the three compartments by 1, 2 and 3, and derive the effective production and loss rates for compartment 1. For $i = 2, 3$, we let $s_i$ be the *survival* probability that a monomer entering compartment $i$ eventually makes it to compartment 1. We also define the total exit rate from compartments 2 and 3 as $h_2 = r_{21} + r_{23} + l_2$ and $h_3 = r_{31} + r_{32} + l_3$, respectively. To calculate the effective production and loss rates for compartment 1, we need to derive the unknown survival probabilities $s_2$ and $s_3$. By Figure 1, it follows that

$$s_2 = \frac{r_{21}}{h_2} + \frac{r_{23}}{h_2} s_3, \tag{5}$$

$$s_3 = \frac{r_{31}}{h_3} + \frac{r_{32}}{h_3} s_2. \tag{6}$$

For example, equation (5) states that the probability that a monomer entering compartment 2 makes it to compartment 1 equals the probability that it goes directly to compartment 1 ($\frac{r_{21}}{h_2}$) plus the probability that it first goes to compartment 3 ($\frac{r_{23}}{h_2}$) and from there eventually makes it to compartment 1 ($s_3$). The solution to

equations (5)-(6) is

$$s_2 = \left(\frac{r_{21}}{h_2} + \frac{r_{23}r_{31}}{h_2h_3}\right)\left(1 - \frac{r_{23}r_{32}}{h_2h_3}\right)^{-1}, \tag{7}$$

$$s_3 = \left(\frac{r_{31}}{h_3} + \frac{r_{32}r_{21}}{h_2h_3}\right)\left(1 - \frac{r_{23}r_{32}}{h_2h_3}\right)^{-1}. \tag{8}$$

With the survival probabilities in hand, the effective production and loss rates are given by

$$\hat{p}_1 = p_1 + p_2s_2 + p_3s_3, \tag{9}$$

$$\hat{l}_1 = l_1 + r_{12}(1 - s_2) + r_{13}(1 - s_3). \tag{10}$$

Note that the effective production rate of compartment 1 is enhanced by the survival of monomers in other compartments, whereas the effective loss rate of compartment 1 is increased by the $1 - s$ terms, i.e., by the monomers that are transported from compartment 1 to the other compartments but never return.

We define the effective production and loss rates in the brain, $\hat{p}_b$ and $\hat{l}_b$, by substituting $b$ for 1, $c$ for 2 and $p$ for 3 (or, by symmetry, $p$ for 2 and $c$ for 3) in the subscripts of equations (9) and (10). Similarly, the effective rates for CSF (plasma, respectively) are given by substituting $c$ ($p$, respectively) for 1 and the other two compartment subscripts for 2 and 3 in equations (9)-(10).

We are now in a position to present the steady-state solution. To do so, we define the polymerization ratio

$$r = \frac{\hat{p}_b e}{\hat{l}_b f}, \tag{11}$$

which is a unitless quantity that succinctly captures the four key processes of (effective) production, elongation, (effective) loss and fragmentation. Setting the left side of equations (1)-(4) to zero and solving for the steady-state concentrations reveal that there are two regimes: a steady-state (or subcritical) regime where $r < 1$ and a supercritical regime where $r > 1$. In the former case, the A$\beta$ levels eventually attain finite equilibrium values, where

$$b_1 = \frac{\hat{p}_b}{\hat{l}_b}, \tag{12}$$

$$b_i = 2b_1 r^{i-1}, \quad i = 2, 3, \ldots, \tag{13}$$

$$c = \frac{\hat{p}_c}{\hat{l}_c}, \tag{14}$$

$$p = \frac{\hat{p}_p}{\hat{l}_p}. \tag{15}$$

By equations (12)-(13), the total A$\beta$ concentration in the brain (i.e., the total number of A$\beta$ molecules, whether they exist as monomers or as part of polymers), which is denoted by $b = \sum_{i=1}^{\infty} ib_i$, is

$$b = \frac{\hat{p}_b}{\hat{l}_b}\left(\frac{2}{(1-r)^2} - 1\right). \tag{16}$$

There are several noteworthy features of our steady-state solution. First, the steady-state A$\beta$ levels in the plasma ($p$), the CSF ($c$), and the brain monomers ($b_1$) are linear and increasing in compartment production terms, and independent of the elongation rate $e$ and the fragmentation rate $f$; these latter two parameters only affect the brain $i$-mer concentration for $i \geq 2$. All steady-state concentrations are also decreasing in loss rates. The influence of transport parameters on the A$\beta$ levels is more subtle, as explained in the Discussion.

By (16), the brain A$\beta$ burden goes to infinity as the polymerization ratio $r$ approaches 1. If we assume no transport across compartments (i.e., $r_{ij} = 0$ for all $i, j$), then the solution coincides with our one-compartment results[13]. The relatively steady A$\beta$ levels in AD patients[26–28] suggest that the $r < 1$ regime is the clinically relevant one, and that the slow A$\beta$ accumulation in the brain results from a quasi-steady-state situation, where the polymerization ratio $r$ is less than 1 but is slowly increasing over the years. Consequently, the paper focuses on the $r < 1$ regime, and a brief discussion of the $r > 1$ regime is deferred until later.

## Post-treatment kinetics

The impact of treatment can be assessed by changing the appropriate parameter (i.e., production, loss, transport, elongation or fragmentation rate) in the model

and substituting it into equations (14)-(16) to find the post-treatment steady state. To analyze the A$\beta$ kinetics immediately after treatment, we make two simplifying assumptions. The first assumption, which is based on the observation from numerical simulations[13] that the total number of brain oligomers changes much more slowly than the number of monomers, is that the total number of oligomers in the brain, $\sum_{i=2}^{\infty} b_i$, remains constant immediately after treatment; we denote this quantity by $B_2$, which equals $2\frac{\hat{p}_b}{\hat{l}_b}\left(\frac{r}{1-r}\right)$ by equation (13). Under this assumption, the brain monomer level after treatment quickly reaches a new level and thereafter changes much more gradually. This new level, $\bar{b}_1$, is approximated by setting the left side of equation (1) to zero and solving equations (1), (3) and (4) for $b_1$. For ease of presentation, we present the solution for $\bar{b}_1$ under the special case of the parameter values in Table 1 (i.e., $r_{bp} = r_{cb} = r_{pc} = p_c = p_p = l_c = 0$):

$$\bar{b}_1 = \frac{-(\hat{l}_b + eB_2) + \sqrt{(\hat{l}_b + eB_2)^2 + 8e(\hat{p}_b + fB_2)}}{4e}. \tag{17}$$

In equation (17), $B_2$ is the pre-treatment number of oligomers and the four polymerization parameters represent the post-treatment values. Because the rate of intercompartmental exchange (Table 1) is faster than the changes in the brain A$\beta$ polymers after treatment, we make the second simplifying assumption that the steady-state relationships in equations (14)-(15) actually hold for all times after treatment. Therefore, we predict that the CSF and plasma levels rapidly change to (again, assuming the parameters in Table 1)

$$\bar{c} = \frac{r_{bc}\bar{b}_1}{r_{cp} + l_c}, \tag{18}$$

$$\bar{p} = \frac{p_p + \frac{r_{cp}r_{bc}\bar{b}_1}{r_{cp}+l_c}}{r_{pb} + l_p}, \tag{19}$$

respectively, and then gradually approach their post-treatment steady states.

## Parameter estimation

Our model has 10 parameters, which are listed along with their values in Table 1. The value of the A$\beta$ monomer loss rate $l$ in Table 1 corresponds to a half-life of 41.6 minutes, which is close to the crude experimental value of 38 minutes reported by one group in the brains of APP transgenic mice[6]. Protofibrils[29], fibrils[30, 31] and plaques[32] appear to grow primarily via A$\beta$ monomer addition, and we use an elongation rate $e$ in Table 1 taken from a synthetic fibril analysis[31], which is within a factor of two of other estimates for fibrils[30] and protofibrils[29]. For lack of data to the contrary, we set the CSF production rate $p_c$, the CSF loss rate $l_c$ and the plasma production rate $p_p$eq ual to zero.

We assume that only three of the six possible exchanges have a positive transport rate. In particular, we ignore brain→plasma, plasma→CSF and CSF→brain, and assume there is a circular flow given by brain→CSF→plasma→brain. To justify these inclusions and omissions, we note that CSF→brain and brain→plasma transport are likely to be by passive diffusion and these transport rates are probably much smaller than the plasma→brain transport rate, which passes through the BBB according to a saturable mechanism that follows the Michaelis-Menten kinetics, consistent with a specific transport mechanism that dwarfs passive diffusion[8, 9]. Similarly, CSF→plasma transport is quite rapid[10], whereas plasma→CSF transport is difficult because proteins do not readily pass through ultrafiltration[33]. Also, neuronally-produced A$\beta$ is drained/transported into the CSF of mice[34], and hence the brain→CSF flow is included in the model. Our estimate of the transport rate $r_{pb}$ is taken from studies of guinea pigs[8, 9], and the value for the transport rate $r_{cp}$ is based on a CSF study of rats[10].

This leaves four unknown parameter values, which are determined by solving four equations (using equations (12) and (14)-(16)): the total A$\beta_{42}$ level in the brain $b$ is $1975\times10^3$ pM (averaged over 5 different cortical regions of wet brain tissue of patients with a clinical dementia rating (CDR) score of 5.0 (severe dementia)[35],

assuming that the density of wet cortical tissue is equal to that of water); the CSF A$\beta_{42}$ level $c$ is 115 pM[36]; the plasma A$\beta_{42}$ level is 29 pM[37]; and the fraction of brain A$\beta$ that consists of monomers, $\frac{b_1}{b}$, is 1.3%[38, 39]. These estimates, which are given in Table 1, lead to the polymerization ratio estimate $r = 0.84$.

| Parameter | Description | Value |
|---|---|---|
| $p_b$ | Production rate of brain monomers | $7.34 \times 10^{-12}$ M sec$^{-1}$ |
| $l_b$ | Loss rate constant for brain monomers | 1 hr$^{-1}$ |
| $e$ | Elongation rate constant | 90 M$^{-1}$ sec$^{-1}$ |
| $f$ | Fragmentation rate constant | $2.76 \times 10^{-6}$ sec$^{-1}$ |
| $p_c$ | Production rate of CSF monomers | 0 |
| $l_c$ | Loss rate constant for CSF monomers | 0 |
| $p_p$ | Production rate of plasma monomers | 0 |
| $l_p$ | Loss rate constant for plasma monomers | $6.7 \times 10^{-3}$ sec$^{-1}$ |
| $r_{bc}$ | Transport rate constant for brain→CSF | $7.6 \times 10^{-6}$ sec$^{-1}$ |
| $r_{cp}$ | Transport rate constant for CSF→plasma | $1.7 \times 10^{-3}$ sec$^{-1}$ |
| $r_{pb}$ | Transport rate constant for plasma→brain | $3.77 \times 10^{-5}$ sec$^{-1}$ |
| $r_{bp}$, $r_{pc}$, $r_{cb}$ | Other transport rate constants | 0 |

Table 1: Parameter values for the model.

## Effect of treatment

To assess the impact of a $\gamma$-secretase inhibitor, we numerically solve equations (1)-(4) assuming that a symptomatic patient is in a pre-treatment steady-state on days 0-100, and is administered a $\gamma$-secretase inhibitor that decreases the A$\beta$ production rate $p_b$ by 40% (this modest reduction reflects the potentially adverse effect of a $\gamma$-secretase inhibitor on Notch signalling[40-41]) on days 100-465 (i.e., for 1 year). Figure 2 shows the A$\beta$ dynamics for the brain monomers and for all three compartments. As predicted by equation (15) with the A$\beta$ plasma production rate $p_p$

set equal to zero (details not shown), the monomer levels in the brain and CSF are directly proportional to each other in Figures 2b and 2c. The A$\beta$ concentrations in the CSF and plasma drop to the values predicted in equations (18) and (19) within hours after treatment, and then slowly approach their post-treatment steady states. Note that in this case the values in equations (18) and (19) are very similar to the post-treatment steady-state values. Hence, the CSF and plasma compartments approach their post-treatment steady-state A$\beta$ levels much faster than the brain compartment. The post-treatment steady states represent an 18-fold reduction in the brain, a 1.67-fold reduction in the CSF and a 1.67-fold reduction in the plasma. Upon the discontinuation of treatment, similar kinetics occur: a rapid change in the monomer levels in all three compartments, followed by a slow return to the pre-treatment steady state.

Figure 3 depicts the impact of an agent that enhances fragmentation by 100%. While the steady-state A$\beta$ burden in the brain drops 15.6-fold, the CSF and plasma A$\beta$ levels experience a transient rise and then return to the pre-treatment levels. The return to pre-treatment levels follows from the fact that the fragmentation rate does not alter the steady-state brain monomer level in equation (12), which is the brain's only interaction with the CSF and plasma compartments. In contrast to the case of the production inhibitor in Figure 2, the values in equations (18) and (19) are quite different than the post-treatment steady-state levels in the CSF and plasma. As a result, the rate of approach to steady state is similar for all three compartments.

We now consider an alternative to equations (1)-(4), in which the "all fragmentations" term is deleted from equation (1) and the fragmentation rate is interpreted as the rate of monomer ingestion off of oligomers. Figure 4 shows the impact of an A$\beta$ vaccine[2] that increases the ingestion rate by 100%. In this case, the CSF and plasma levels rise monotonically to post-treatment steady states that are 2.5% higher than the pre-treatment steady states, even though the steady-state brain A$\beta$ burden decreases 8.6-fold.

Finally, we investigate the impact of changing the transport rates. Two possible improvements for reducing the A$\beta$ burden in the brain are to increase the brain$\rightarrow$CSF transport rate, $r_{bc}$, and to decrease the plasma$\rightarrow$brain rate, $r_{pb}$. Figure 6 shows that increasing $r_{bc}$ by 100% causes a modest 17% decrease in the brain A$\beta$ level after one year (the post-treatment steady state level represents a 24% reduction), while almost doubling the A$\beta$ levels in the CSF and plasma. In contrast, a 100-fold reduction in $r_{pb}$ reduces the brain A$\beta$ burden by less then 0.2%.

### Supercritical regime

We now turn to the case where the polymerization ratio $r$ satisfies $r > 1$. A mathematical analysis of this case shows that the A$\beta$ burden in the brain grows without bound, eventually increasing linearly at rate $\hat{p}_b(r-1)/r$ (Figure 5a). The polymer concentrations in the brain are not geometrically distributed as in the $r < 1$ case, but are uniformly distributed, where each $i$-mer successively achieves the concentration $b_1 = f/e$, $b_i = 2f/e$ for $i \geq 2$. Interestingly, the CSF and plasma concentrations attain finite levels in the $r > 1$ case, even though the total brain concentration is unbounded. This is because the brain A$\beta$ burden grows by accumulating larger polymers, not more monomers.

## Discussion

Despite the existence of some mathematical models for A$\beta$ fibrillization and plaque growth, this paper appears to represent the first attempt to use a mathematical model to assess the effect of AD treatment on A$\beta$ levels in various compartments of the body. We provide simple formulas for the steady-state A$\beta$ levels in the brain, CSF and plasma, both before and after treatment. Our solution reveals that there are two possible regimes, depending upon the value of the polymerization ratio in the brain, $r = \frac{\hat{p}_b e}{l_b f}$, which is the product of the effective production rate and elon-

gation rate divided by the product of the effective loss rate and the fragmentation rate. The effective production and loss rates account not just for actual production and loss in the brain, but also for sources and sinks due to transport to and from the plasma and CSF. When the polymerization ratio is less than 1, steady-state A$\beta$ levels are achieved throughout the body. We believe that this is the clinically relevant regime, in light of the slow accumulation of A$\beta$ throughout the body. If $r > 1$, then the A$\beta$ burden in the brain grows indefinitely (by accumulating larger polymers while maintaining a constant monomer level), eventually increasing linearly at rate $\hat{p}_b(r-1)/r$, whereas the A$\beta$ levels in the CSF and plasma remain in a steady state. This unusual state of affairs in the $r > 1$ case is due to two important assumptions in our model: only monomers pass between compartments and no polymerization occurs in the CSF and plasma. Consequently, the brain A$\beta$ interacts with the plasma and CSF only via A$\beta$ monomers.

Consequently, from a biomarker viewpoint, CSF and plasma A$\beta$ levels provide a reliable indirect estimate of the A$\beta$ monomer level in the brain, but not necessarily of the total A$\beta$ burden in the brain. An extreme example of this is the $r > 1$ case above, where the easily-monitored CSF and plasma levels remain constant and do not hint at the unbounded A$\beta$ accumulation in the brain. However, our analysis also has implications for the monitoring and assessment of treatment. Agents that inhibit the production of A$\beta$ monomers[5, 6] or increase the monomer loss rate in the brain are likely to cause significant reductions in the A$\beta$ levels in all three compartments, with the CSF and plasma compartments attaining their post-treatment steady-state levels more quickly than the brain. In contrast, agents that ingest monomers off of polymers[2], reduce the elongation rate, or increase the fragmentation rate of A$\beta$ polymers in the brain, may cause only minor changes – including increases – in the steady-state CSF and plasma levels, which are not indicative of their impact on the total A$\beta$ burden in the brain. However, if soluble A$\beta$ monomers are the primary toxic moiety[38, 42], then the plasma A$\beta$ and CSF A$\beta$ levels may be excellent

biomarkers for all Alzheimer's treatments, and production inhibitors may be more efficacious than other agents that have less impact on A$\beta$ monomers. The prevention of cognitive impairment in mice by an A$\beta$ vaccine[7] suggests that this may not be the case.

Our analysis also reveals how the transport parameters affect the distribution of A$\beta$ throughout the body. The relationship of A$\beta$ levels to transport parameters is more subtle. For example, a drug that increases removal of A$\beta$ from the brain by increasing the transport rate to the CSF (a possible mechanism of the Elan vaccine[2]) will increase the CSF A$\beta$ level but the change in plasma A$\beta$ level can be positive or negative, depending on the relative contributions to plasma monomers by the brain ($b_1 r_{bp}$), which will fall, and the CSF ($c r_{cp}$), which will rise. With the parameters chosen in this paper (based on A$\beta_{42}$), the plasma level rises because the CSF rather than the brain is the primary extra-compartmental source of plasma A$\beta$. However, in the case of A$\beta_{40}$, where it is estimated that $r_{bp}$ is 10 times larger than $r_{bc}$[43], our analysis indicates that plasma A$\beta_{40}$ levels would decrease as a consequence of such a therapy.

While many of the model's parameter values are imprecisely known and the model is rather simple (e.g., first-order transport, linear relationship between free and bound A$\beta$), the qualitative nature of our results should be robust because they stem in large part from the empirical observation[21] that very few A$\beta$ polymers reside in the CSF or plasma, suggesting that A$\beta$ polymerization occurs almost exclusively in the brain and A$\beta$ polymers are not easily transported out of the brain. However, as was done in HIV research [44, 45], mathematical analysis such as this can be combined with data generated by perturbation of human A$\beta$ compartments by novel agents to derive estimates of some parameters that are difficult to measure *in vivo*, thereby uncovering the primary flow dynamics of A$\beta$ in the body. More generally, our model provides a systematic framework with which to interpret upcoming human clinical trials of novel agents for Alzheimer's disease.

**Acknowledgment**

This research was partially supported by the Singapore-MIT Alliance (LMW) and by the Foundation for Neurologic Diseases (DJS).

## References


[1] Selkoe, D. J. Translating cell biology into therapeutic advances in Alzheimer's disease. *Nature* **399 (Supp)**, A23-A31 (1999).

[2] Schenk, D., Barbour, R., Dunn, W., Gordon, G., Grajeda, H., Guido, T., Hu, K., Huang, J. Johnson-Wood, K., Khan, K., Kholodenko, D., Lee, M., Liao, Z., Lieberburg, I., Motter, R., Mutter, L., Soriano, F., Shopp, G., Vasquez, N., Vandevert, C., Walker, S., Wogulis, M., Yednock, T., Games, D. & Seubert, P. Immunization with amyloid-$\beta$ attenuates Alzheimer-disease-like pathology in the PDAPP mouse. *Nature* **400**, 173-177 (1999).

[3] Bard, F., Cannon, C., Barbour, R., Burke, R.-L., Games, D., Grajeda, H., Guido, T., Hu, K., Huang, J., Johnson-Wood, K., Khan, K., Kholodenko, D., Lee, M., Lieberburg, I., Motter, R., Nguyen, M., Soriano, F., Vasquez, N., Weiss, K., Welch, B., Seubert, P., Schenk, D. & Yednock, T. Peripherally administered antibodies against amyloid $\beta$-peptide enter the central nervous system and reduce pathology in a mouse model of Alzheimer disease. *Nature Medicine* **6** 916-919 (2000).

[4] Weiner, H. L., Lemere, C. A., Maron, R., Spooner, E. T., Grenfell, T. J., Mori, C., Issazadeh, S., Hancock, W. W. & Selkoe, D. J. Nasal administration of amyloid-beta peptide decreases cerebral amyloid burden in a mouse model of Alzheimer's disease. *Ann. Neurol.* **48**, 567-579 (2000).

[5] Wolfe, M. S., Xia, W., Moore, C. L., Leatherwood, D. D., Ostaszewski, B. L., Rahmati, T., Donkor, I. O. & Selkoe, D. J. Peptidomimetic probes and molecular modeling suggest Alzheimer's $\gamma$-secretase is an intramembrane-cleaving aspartyl protease. *Biochem.* **38**, 4720-4727 (1999).

[6] Felsenstein, K. M. The next generation of AD therapeutics: the future is now. *Abstracts from the 7th annual conference on Alzheimer's disease and related disorders*, Abstract 613 (2000).

[7] Janus, C., Pearson, J., McLaurin, J., Mathews, P. M., Jiang, Y., Schmidt, S. D., Chisti, M. A., Horne, P., Heslin, D., French, J., Mount, H. T. J., Nixon, R. A., Mercken, M., Bergeron, C., Fraser, P. E., St. George-Hyslop, P. & Westaway, D. A$\beta$ peptide immunization reduces behavioral impairment and plaques in a model of Alzheimer's disease. *Nature* **408**, 979-982 (2000).

[8] Zlokovic, B. V., Ghiso, J., Mackic, J. B., McComb, J. G., Weiss, M. H. & Frangione, B. Blood-brain barrier transport of circulating Alzheimer's amyloid $\beta$. *Biochem. Biophys. Res. Comm.* **197**, 1034-1040 (1993).

[9] Martel, C. L., Mackic, J. B., McComb, J. G., Ghiso, J. & Zlokovic, B. V. Blood-brain barrier uptake of the 40 and 42 amino acid sequences of circulating Alzheimer's amyloid $\beta$ in guinea pigs. *Neuroscience Letters* **206**, 157-160, 1996.

[10] Ghersi-Egea, J.-F., Gorevic, P. D., Ghiso, J., Frangione, B., Patlak, C. S. & Fenstermacher, J. D. Fate of cerebrospinal fluid-borne amyloid $\beta$-peptide: rapid clearance into blood and appreciable accumulation by cerebral arteries. *J. Neurochemistry* **166**, 880-883, 1996.

[11] Poduslo, J. F., Curran, G. L., Haggard, J. J., Biere, A. L. & Selkoe, D. J. Permeability and residual plasma volume of human, Dutch variant, and rat amyloid $\beta$-protein 1-40 at the blood-brain barrier. *Neurobiol. Dis.* **4**, 27-34, 1997.

[12] Mackic, J. B., Weiss, M. H., Miao, W., Kirkman, E., Ghiso, J., Calero, M., Bading, J., Frangione, B. & Zlokovic, B. V. Cerebrovascular accumulation and increased blood-brain barrier permeability to circulating Alzheimer's amyloid

$\beta$ peptide in aged squirrel monkey with cerebral amyloid angiopathy. *J. Neurochem.* **70**, 210-215, 1998.

[13] Craft, D. L., Wein, L. M. & Selkoe, D. J. The impact of novel treatments on A$\beta$ burden in Alzheimer's disease: insights from a mathematical model. Submitted for publication, 2001.

[14] Lemere, C. A., Blusztajn, J. K., Yamaguchi, H., Wisniewski, T., Saido, T. C. & Selkoe, D. J. Sequence of deposition of heterogeneous amyloid $\beta$-peptides and APO E in down syndrome: implications for initial events in amyloid plaque formation. *Neurobiol. Dis.* **3**, 6-12, 1996.

[15] Oyler, G. A., Duckrow, R. B. & Hawkins, R. A. Computer simulation of the blood-brain barrier: a model including two membranes, blood flow, facilitated and non-facilitated diffusion. *J. Neurosc. Meth.* **44**, 179-196, 1992.

[16] Gravina, S. A., Ho, L., Eckman, C. B., Long, K. E., Otvos, L. Jr., Younkin, L. H., Suzuki, N. & Younkin, S. G. Amyloid $\beta$ (A$\beta$) in Alzheimer's Disease Brain: biochemical and immunocytochemical analysis with antibodies specific for forms ending at A$\beta$40 or A$\beta$42(43). *Journal of Biochemistry* **270**, 7013-7016 (1995).

[17] Oosawa, F. & Kasai, M. Actin. A theory of linear and helical aggregations of macromolecules. *J. Mol. Biol.* **4**, 10-21, 1962.

[18] Flory, P. J. *Principles of polymer chemistry.* Cornell University Press, Ithaca, NY, 1953.

[19] von Smoluchowski, M. Drei vorträge über diffusion, brownsche bewegung und koagulation von kolloidteilchen. *Z. Phys.* **17**, 557-585 (1916).

[20] von Smoluchowski, M. Versuch einer mathematischen theorie der koagulationskinetic kolloider lösungen. *Z. Phys.* **92**, 129-168 (1917).

[21] Walsh, D. M., Tsang, B. P., Rydel, R. E., Podlisny, M. B. & Selkoe, D. J. The oligomerization of amyloid $\beta$-protein begins intracellularly in cells derived from human brain. *Biochemistry* **39**, 10831-10839, 2000.

[22] Lutz, R. J., Dedrick, R. L. & Zaharko, D. S. Physiological pharmacokinetics: an *in vivo* approach to membrane transport. *Pharmac. Ther.* **11**, 559-592 (1980).

[23] Kuo, Y.-M., Emmerling, M. R., Lampert, H. C., Hempelman, S. R., Kokjohn, T. A., Woods, A. S., Cotter, R. J. & Roher, A. E. High levels of circulating A$\beta$42 are sequestered by plasma proteins in Alzheimer's disease.

[24] Biere, A. L., Ostaszewski, B., Stimson, E. R., Hyman, B. T., Maggio, J. E. & Selkoe, D. J. Amyloid $\beta$-peptide is transported on lipoproteins and albumin in human plasma. *J. Biol. Chem.* **271**, 32916-32922 (1996).

[25] Chauhan, V. P. S., Ray, I., Chauhan, A. & Wisniewski, H. M. Binding of gelsolin, a secretory protein, to amyloid $\beta$-protein. *Biochem. Biophys. Res. Comm.* **258**, 241-246, 1999.

[26] Hyman, B. T. Marzloff, K & Arriagada, P. V. The lack of accumulation of senile plaques or amyloid burden in Alzheimer's disease suggests a dynamic balance between amyloid deposition and resolution. *J. Neuropathol. Exp. Neurol.* **52**, 594-600 (1993).

[27] Arriagada, P. V., Growdon, J. H., Hedley-Whyte, E. T. & Hyman, B. T. Neurofibrillary tangles but not senile plaques parallel duration and severity of Alzheimer disease. *Neurology* **42**, 631-639 (1992).

[28] Berg, L., McKeel, D. W., Miller, J. P., Baty, J. & Morris, J. C. Neuropathological indexes of Alzheimer's disease in demented and nondemented persons aged 80 years and older. *Arch. Neurol.* **50** 349-358 (1993).

[29] Harper, J. D., Wong, S. S., Lieber, C. M. & Lansbury, P. T. Jr. Assembly of A$\beta$ Amyloid protofibrils: an *in vitro* model for a possible early event in Alzheimer's disease. *Biochemistry* **38**, 8972-8980 (1999).

[30] Lomakin, A., Chung, D. S., Benedek, G. B., Kirschner, D. A. & Teplow, D. B. On the nucleation and growth of amyloid $\beta$-protein fibrils: detection of nuclei and quantitation of rate constants. *Proc. Natl. Acad. Sci. USA* **93**, 1125-1129 (1996).

[31] Lomakin, A., Teplow, D. B., Kirschner, D. A. & Benedek, G. B. Kinetic theory of fibrillogenesis of amyloid $\beta$-protein *Proc. Natl. Acad. Sci. USA* **94**, 7942-7947 (1997).

[32] Tseng, B. P., Esler, W. P., Clish, C. B., Stimson, E. R., Ghilardi, J. R., Vinters, H. V., Mantyh, P. W., Lee, J. P. & Maggio, J. E. Deposition of monomeric, not oligomeric, A$\beta$ mediates growth of Alzheimer's disease amyloid plaques in human brain preparations. *Biochemistry* **38**, 10424-10431 (1999).

[33] Betz, A. L., Goldstein, G. W. & Katzman, R. Blood-brain-cerebrospinal fluid barriers. Chapter 30 of *Basic neurochemistry: molecular, cellular, and medical aspects, 4th Ed.*, ed. Siegel, G. J., Raven Press, Ltd., New York, 1989.

[34] Calhoun, M. E., Burgermeister, P., Phinney, A. L., Stalder, M., Tolnay, M., Wiederhold, K.-H., Abramowski, D., Sturchler-Pierrat, C., Sommer, B., Staufenbiel, M. & Jucker, M. Neuronal overexpression of mutant amyloid precursor protein results in prominent deposition of cerebrovascular amyloid. *Neurobiology* **96**, 14088-14093, 1999.

[35] Näslund, J., Haroutunian, V., Mohs, R., Davis, K. L., Davies, P., Greengard, P. & Buxbaum, J. D. Correlation between elevated levels of amyloid $\beta$-peptide in the brain and cognitive decline. *JAMA* **283**, 1571-1577 (2000).

[36] Galasko, D., Chang, L., Motter, R., Clark, C. M., Kaye, J., Knopman, D., Thomas, R., Kholodenko, D., Schenk, D., Lieberburg, I., Miller, B., Green, R., Basherad, R., Kertiles, L., Boss, M. A. & Seubert, P. High cerebrospinal fluid tau and low amyloid $\beta 42$ levels in the clinical diagnosis of Alzheimer disease and relation to Apolipoprotein E genotype. *Arch. Neurol.* **55**, 937-945 (1998).

[37] Scheuner, D., Eckman, C., Jensen, M. Song, X., Citron, M., Suzuki, N., Bird, T. D., Hardy, J., Hutton, M., Kukull, W., Larson, E., Levy-Lahad, E., Viitanen, M., Peskind, E., Poorkaj, P., Schellenberg, G., Tanzi, R., Waco, W., Lannfelt, L., Selkoe, D. & Younkin, S. *Nature Medicine* **2**, 864-870, 1996.

[38] McLean, C. A., Cherny, R. A., Fraser, F. W., Fuller, S. J., Smith, M. J., Beyreuther, K., Bush, A. I. & Masters, C. L. Soluble pool of A$\beta$ amyloid as a determinant of severity of neurodegeneration in Alzheimer's disease. *Ann Neurol* **46**, 860-866 (1999).

[39] Wang, J., Dickson, D. W., Trojanowski, J. Q. & Lee, V. M.-Y. The levels of soluble versus insoluble brain A$\beta$ distinguish Alzheimer's disease from normal and pathologic aging. *Experimental Neurology* **158**, 328-337 (1999).

[40] Wolfe, M. S., Xia, W., Ostaszewski, B. L., Diehl, T. S., Kimberley, W. T., & Selkoe, D. J. Two transmembrane aspartates in presenilin-1 required for presenilin endoproteolysis and $\gamma$-secretase activity. *Nature* **398**, 513-517 (1999).

[41] Ye, Y., Lukinova, N. & Fortini, M. E. Neurogenic phenotypes and altered Notch processing in Drosophila Presinilin mutants. *Nature* **398**, 525-529 (1999).

[42] Lue, L.-F., Kuo, Y.-M., Roher, A. E., Brachova, L., Shen, Y., Sue, L., Beach, T., Kurth, J. H., Rydel, R. E. & Rogers, J. Soluble amyloid $\beta$ peptide concentration as a predictor of synaptic change in Alzheimer's disease. *Am. J. Pathol.* **155**, 853-862 (1999).

[43] Shibata, M., Yamada, S., Kumar, S.R., Calero, M., Bading, J., Frangione, B., Holtzman, D.M., Miller, C.A., Strickland, D.K., Ghiso, J. & Zlokovic, B.V., Clearance of Alzheimer's amyloid-ss(1-40) peptide from brain by LDL receptor-related protein-1 at the blood-brain barrier. *J. Clin. Invest.* **106(12)**, 1489-1499 (2000).

[44] Wei X., Ghosh S.K., Taylor M.E. Johnson VA, Emini, E.A., Deutsch, P., Lifson, J.D., Bonhoffer, S., Nowak, M.A., Hahn, B.H. & Shaw, G. Viral dynamics in human immunodeficiency virus type 1 infection. *Nature* **373**, 117-123 (1995).

[45] Ho D.D., Neumann A.U., Perelson A.S., Chen W., Leonard J.M. & Markowitz M. Rapid turnover of plasma virions and CD4 lymphocytes in HIV-1 infection. *Nature* **373**, 123-126 (1995).

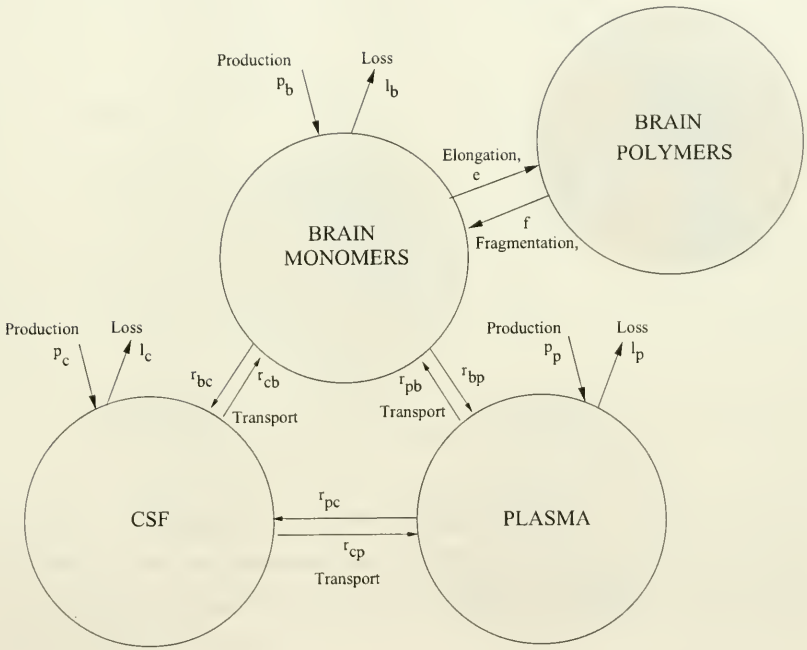


Figure 1: A pictorial depiction of the mathematical model.

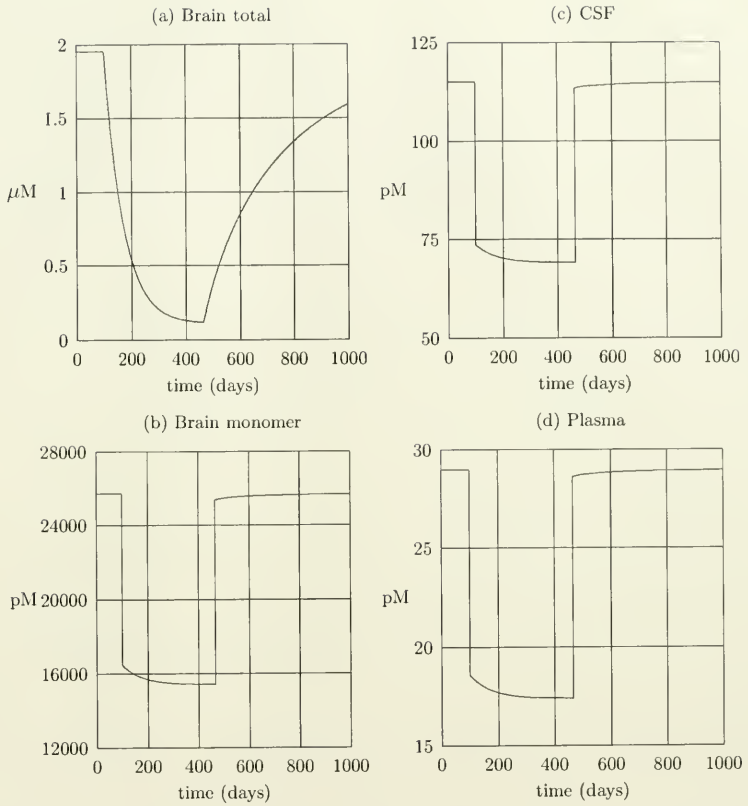


Figure 2: A $\gamma$-secretase inhibitor, which decreases the monomer production rate in the brain by 40%, is administered from day 100 to day 465. The total A$\beta$ burden (a), the brain monomer level (b), the CSF A$\beta$ level (c), and the plasma A$\beta$ level (d) are plotted against time.

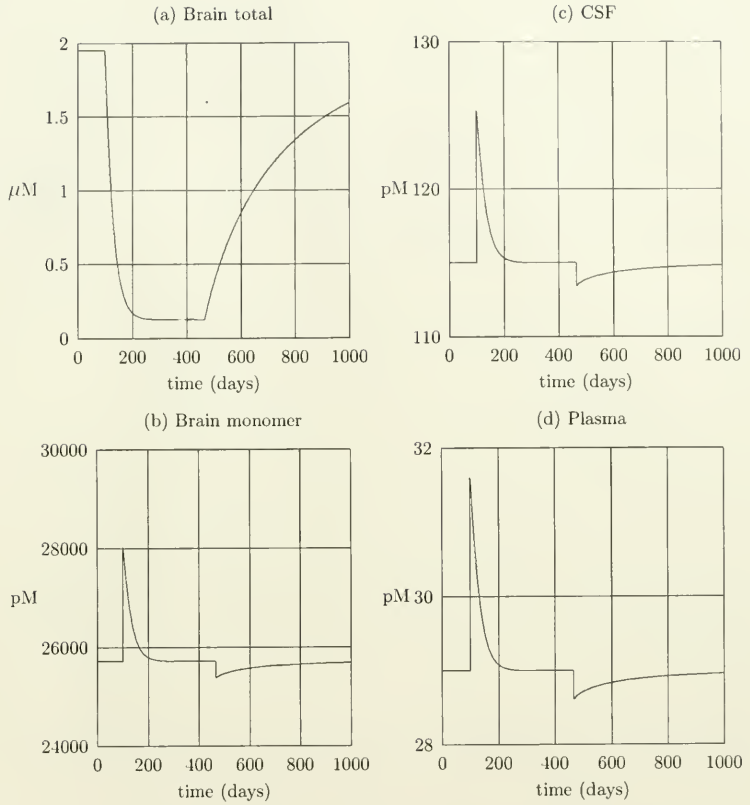


Figure 3: A fragmentation enhancer, which increases the fragmentation rate by 100%, is administered from day 100 to day 465. The total A$\beta$ burden (a), the brain monomer level (b), the CSF A$\beta$ level (c), and the plasma A$\beta$ level (d) are plotted against time.

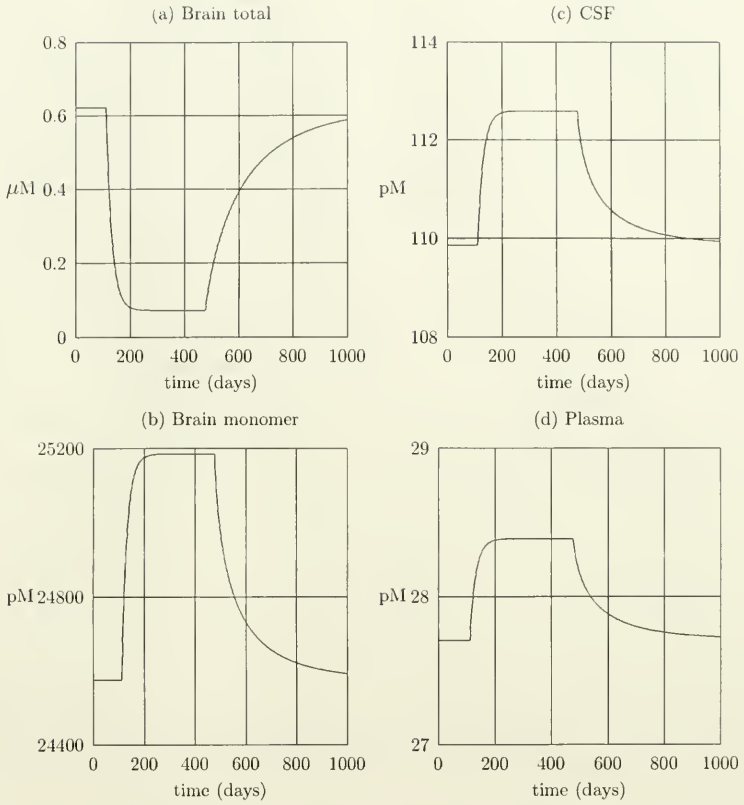


Figure 4: A vaccine, which increases the monomer ingestion rate off of polymers by 100% in our alternative model, is administered from day 100 to day 465. The total A$\beta$ burden (a), the brain monomer level (b), the CSF A$\beta$ level (c), and the plasma A$\beta$ level (d) are plotted against time.

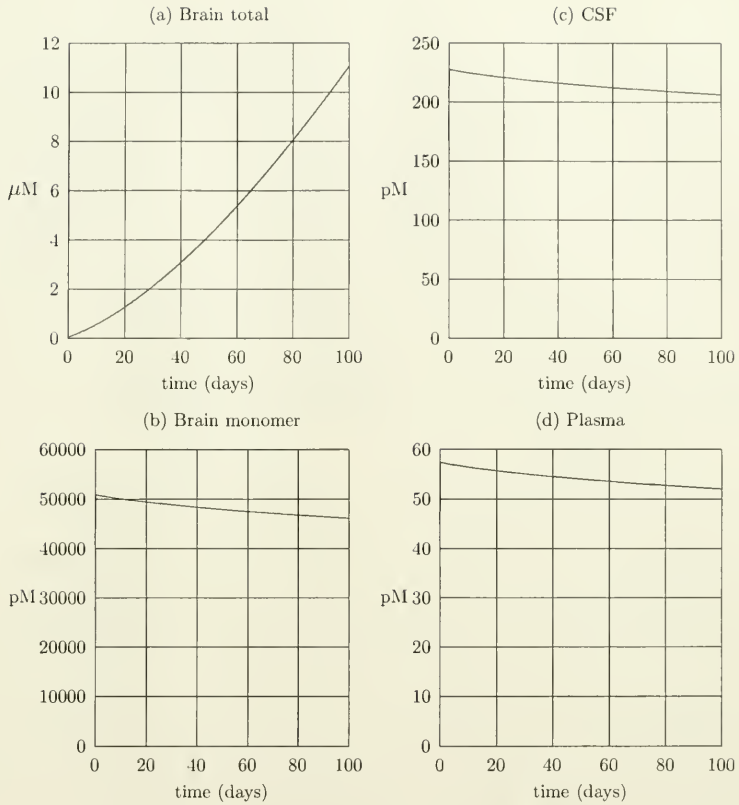


Figure 5: A simulation of equations (1)-(4) when the polymerization ratio $r = 1.007$. The total A$\beta$ burden (a), the brain monomer level (b), the CSF A$\beta$ level (c), and the plasma A$\beta$ level (d) are plotted against time. The slope of the curve in (a) approaches the asymptotic linear growth rate, $\hat{p}(r-1)/r$, while the other three quantities attain finite steady-state levels.

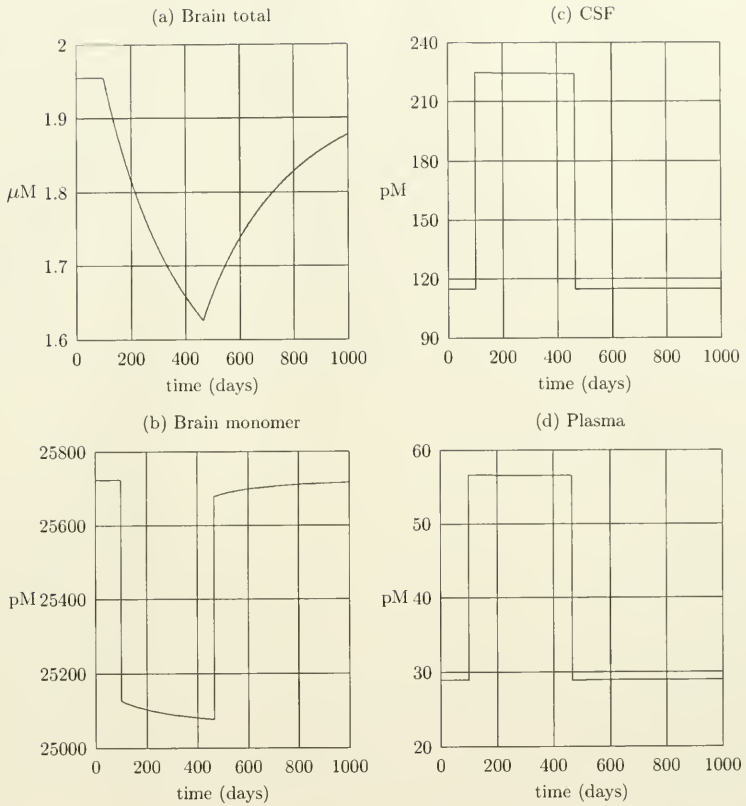


Figure 6: An agent that increases the transport rate from brain to CSF by 100% is administered from day 100 to day 465. The total A$\beta$ burden (a), the brain monomer level (b), the CSF A$\beta$ level (c), and the plasma A$\beta$ level (d) are plotted against time.